Bandwidth Efficient Power Line Communications Based on OFDM

Lutz H.-J. Lampe and Johannes B. Huber

Abstract Power line communications for high data rates using orthogonal frequency division multiplexing are considered. We regard the situations where no channel information is available at the transmitter and where channel information is/ is not provided to the receiver. In order to enable a performance evaluation of transmission schemes with different bandwidth efficiencies, a stochastic representation of the channel transfer function is given, which leads to a fading channel model. As an appropriate measure of performance when applying powerful channel coding, the capacity of this special fading channel is calculated. The combination of a large signal constellation and low rate codes in order to obtain a fixed target rate proves to be advantageous both for coherent and bandwidth efficient noncoherent transmission over power line. The theoretic considerations are affirmed by means of simulations.

Keywords power line communications, OFDM, channel capacity

1. Introduction

The use of the power distribution grid to access world–wide communications networks has attracted much attention and has become a mature subject of research in the last few years. Although the power line network has not been designed for transferring data and is thus characterized by unfavorable transmission properties, frequency ranges of some MHz are at the disposal for telecommunication purposes. To achieve high data rates of some Mbit/s required for multimedia applications, sophisticated and well designed digital transmission systems are necessary in order to exploit the available frequency bands.

In this paper, the well–known multicarrier technique orthogonal frequency division multiplexing (OFDM), e.g. [1], is considered as modulation scheme. By the application of OFDM, the most distinct property of the power line channel, its frequency selectivity, can be easily coped with. Furthermore, OFDM makes a very efficient use of the allocated bandwidth possible [2].

We concentrate on the case where no information about the channel is available at the transmitter side. Starting from a linear system approach of the transmission channel, a stochastic channel model is given. By employing OFDM, a slowly time–varying, frequency non–selective fading channel results for power line communications. Since we assume the application of powerful channel coding schemes, cf. e.g. [3], the capacity of this fading channel is regarded as appropriate measure for performance evaluation. Hence, guidelines for a system design are obtained by calculating the capacity for bandwidth efficient transmission with and with no channel state information at the receiver. In the case of noncoherent reception differential encoding at the transmitter and multiple symbol differential detection at the receiver are proposed [4]. The pos-

sible gain in terms of required signal–to–noise ratio due to perfect channel state information available at the receiver side is quantified. We show that due to the fading the use of relatively large signal constellations in combination with low rate codes [5] is well suited for communication over a large class of power line channels.

The paper is organized as follows: In Section 2 a stochastic representation of the channel transfer function is proposed. The resulting fading channel model for OFDM transmission is presented in Section 3. Section 4 gives the system model and the calculation of capacity for both coherent and noncoherent reception. In Section 5 capacity curves are shown for relevant examples. Section 6 presents simulation results which correspond well to the capacity analysis.

2. Stochastic Power Line Channel Model

Using the power distribution grid for communication purposes the transmission line is appropriately described by a linear, dispersive, time–invariant system, at least for time intervals which are very long compared to the duration of one OFDM–symbol. Thus, the channel is characterized by a channel transfer function $H(f)$ and a subsequent additive noise term. Throughout the paper, $H(f)$ constitutes the transfer function in the equivalent low–pass domain, cf. e.g. [6, Appendix].

2.1 Channel Transfer Function

Due to the structure of typical power line networks with a lot of impedance discontinuities a transmitted signal will be received as a number of distinctively delayed and attenuated signals at the receiver side corresponding to reflections from those discontinuities. Hence, a multi–path signal propagation model seems to be suitable to describe the channel transfer characteristics. Neglecting the (slow) time–variance of the channel (cf. e.g. [7]) this model was used in e.g. [8, 9] for presenting a deterministic expression of $H(f)$ depending on some parameters.

But in many situations, a stochastic model regarding the transfer function as a random process $H(\eta, f)$, where η denotes the atomic event of the random experiment, is desirable instead of one determined transfer function. Clearly, as the signal attenuation and phase on the long term increase with the frequency f, $H(\eta, f)$ is a *non–stationary* random process along the frequency axis. Sample functions of this process are illustrated in Figure 1.

For a certain frequency f the random variable $H(\eta, f)$ results from the superposition of numerous independent random variables which represent the effects of mismatched lines in power line networks. Therefore, the application of the central limit theorem is motivated [10], which yields $H(\eta, f)$ to be a complex *non–stationary Gaussian process* with autocorrelation function (.*: complex conjugation, $\mathcal{E}$ denotes expectation)

$$\phi_{HH}(f_1, f_2) \overset{\triangle}{=} \mathcal{E}\{H(\eta, f_1) * H^*(\eta, f_2)\} \qquad (1)$$

Dipl.–Ing. Lutz H.–J. Lampe, Prof. Dr.–Ing. Johannes B. Huber, Laboratorium für Nachrichtentechnik, Universität Erlangen–Nürnberg, Cauerstraße 7/NT, D–91058 Erlangen, Germany Phone: +49-9131-85-28718, Fax: +49-9131-85-28919, email: llampe@lnt.de
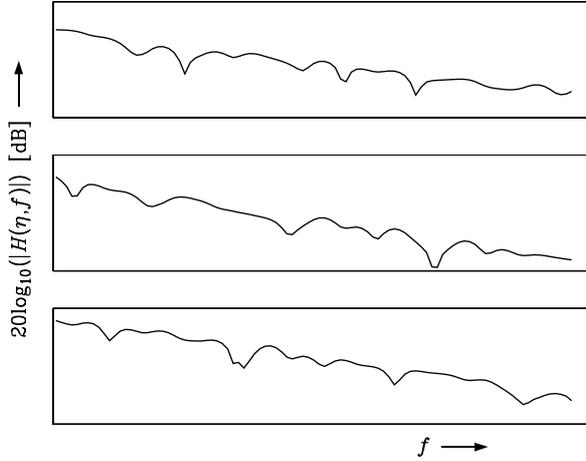
Fig. 1. Sample functions of the non–stationary random process $H(\eta, f)$.

Fig. 2. Example of the autocorrelation function $\phi_{\tilde{H}\tilde{H}}(\Delta f)$ of the random process $\tilde{H}(\eta, f)$ with coherence bandwidth B_c.

and mean value

$$m(f) \triangleq \mathcal{E}\{H(\eta, f)\} \ . \tag{2}$$

We will denote the second moment of the non–stationary process, i.e., the average power of the transfer function, by

$$P(f) \triangleq \phi_{HH}(f, f) = \mathcal{E}\{|H(\eta, f)|^2\} \ . \tag{3}$$

Generally, the average gain $\sqrt{P(f)}$ and the frequency dependent average phase term $\varphi_0(f)$ of the set of transfer functions can be assumed to be characteristic for different types of power line networks and communication links over these networks. The average power transfer function may be approximated by
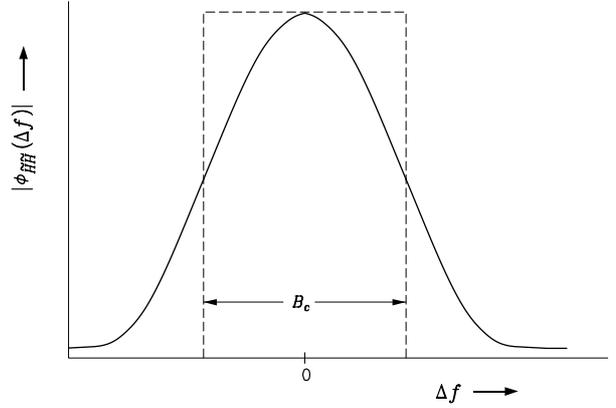
$$P(f) \propto \exp(-a \cdot f) \tag{4}$$

in many situations, where the attenuation parameter a corresponds to different network types. The average phase term can be expressed by

$$\varphi_0(f) = \sum_i c_i f^{b_i}, \tag{5}$$

where c_i are normalization constants, and, for example, terms for $b_i = 0$ correspond to the phase term due to the transformation into the lowpass domain, terms for $b_i = 0.5$ describe the skin–effect, and terms for $b_i = 1$ give the phase term representing the average signal delay. Hence, it is convenient to eliminate these average values and to define a normalized random process

$$\tilde{H}(\eta, f) \triangleq \frac{H(\eta, f)}{\sqrt{P(f)} \cdot e^{-j\varphi_0(f)}} \ . \tag{6}$$

For simplicity, let the mean value of $\tilde{H}(\eta, f)$ be constant over f. If additionally the autocorrelation function (acf) $\phi_{\tilde{H}\tilde{H}}(f + \Delta f, f)$ of this normalized process only depends on the frequency difference Δf, i.e., $\phi_{\tilde{H}\tilde{H}}(f + \Delta f, f) \triangleq$

$\phi_{\tilde{H}\tilde{H}}(\Delta f), \forall f \in \mathbf{R}$, $\tilde{H}(\eta, f)$ is well modeled by a *stationary Gaussian process*. An exemplary acf $\phi_{\tilde{H}\tilde{H}}(\Delta f)$ for this normalized stationary process is depicted in Figure 2. Within the coherence bandwidth B_c which is defined by

$$B_c = \frac{1}{\phi_{\tilde{H}\tilde{H}}(0)} \int_{-\infty}^{\infty} \phi_{\tilde{H}\tilde{H}}(f) \, df \tag{7}$$

the transfer function does not change significantly.

2.2   Additive Noise

In power line communication systems interference of several types occurs, usually categorized in colored noise, impulsive noise, and narrow–band noise, cf. e.g. [11, 12]. However, an adequate representation of the interference scenario has not been given yet. Therefore, we assume the additive Gaussian noise with power spectral density $\Phi_{nn}(f)$. Now, let the normalized channel transfer function $\tilde{H}(\eta, f)$ virtually comprise not only the power lines and the transmitter and receiver filters, but also a noise whitening filter $H_{\mathrm{WF}}(f)$ with the amplitude transfer function

$$|H_{\mathrm{WF}}(f)| = \sqrt{\frac{N_0}{\Phi_{nn}(f)}} \ . \tag{8}$$

Then, the derivations in the previous section remain valid and, as in the subsequent analyses mainly the signal–to–noise ratio (SNR) at the receiver side is considered, we can apply the simple model of additive white Gaussian noise (AWGN) with one–sided noise power spectral density N_0, which is equal to the two–sided spectral noise power density of the equivalent complex baseband white Gaussian noise process.

AEÜ Int. J. El. Commun.
(1999) No. x, 1–1

Lampe, Huber: Bandwidth Efficient Power Line Communications Based on OFDM 3

3. Multicarrier Modulation

On the basis of the introduced stochastic power line channel model, now a simple model for power line communication using orthogonal frequency division multiplexing (OFDM), e.g. [1], is derived. Due to the properties of OFDM, the stochastic process along the frequency axis is transformed into an equivalent *discrete–time process*, which models a *fading* channel.

3.1 Application of OFDM to Power Lines

Core of the OFDM–system is the conversion of the convolution of the transmit signal and the channel impulse response into a component-wise multiplication of samples of their Fourier transforms. For transformation of linear convolution into cyclic convolution, each block of D channel symbols is preceded by the D_0 last symbols of the same block at the transmitter and at the receiver only D symbols out of $D + D_0$ received symbols are taken. D_0 is commonly referred to as guard interval, e.g. [1]. If the guard interval is at least as long as the (discrete–time) channel impulse response, OFDM partitions the dispersive channel into D independent AWGN–subchannels (subcarriers). The subchannel transfer factors λ_ν are samples of the channel transfer function $H(f)$:

$$\lambda_\nu = H(\Delta f \cdot \nu) , \quad \nu = 0, 1, \ldots, D - 1 . \qquad (9)$$

where Δf denotes the OFDM–subcarrier spacing.

Generally, the signal–to–noise ratios in these subchannels differ significantly. Clearly, if the subchannel SNR is known at the transmitter side the transmit power and information rate can be appropriately assigned (loaded) to each subchannel. For that purpose, a number of loading algorithms have been proposed [1, 13, 14, 15]. In power line communication schemes channel state information usually is not available at the transmitter, especially for the point–to–multipoint transmission situations. Thus, loading is not further considered.

Without loading, equal power and equal information rate have to be assigned to the OFDM–subcarriers. If the signal processing is performed independently in each subchannel, only a subset of subcarriers would allow reliable communication. An advantageous alternative is to employ channel coding across the subcarriers. In this case, in the decoding the reliably received symbols from a subchannel with relatively high SNR are used to restore the unreliable symbols from a subchannel with relatively low SNR. In [16] it is shown that for typical flat fading channels almost their capacity is achievable even without loading.

3.2 Fading Channel Model

First, we regard the transmission of only one OFDM–symbol. The signaling along the discrete frequency axis in OFDM is equivalent to transmission over a frequency non–selective (flat) discrete–"time" fading channel. Describing this fading channel in the equivalent low–pass domain [6, Appendix], the complex–valued channel state is related to the subcarrier transfer factors and the channel transfer function, respectively, by ($k \in \mathbf{Z}$: discrete–"time" index)

$$s[k] = \lambda_k = H(\Delta f \cdot k) , \quad k = 0, 1, \ldots, D - 1 . \quad (10)$$

Let $x[k]$ and $y[k]$ denote the fading channel input and output signal, respectively, the input–output–relation reads

$$y[k] = s[k] \cdot e^{j\varphi_c} \cdot x[k] + n[k] , \qquad (11)$$

where φ_c is the carrier phase offset between transmitter and receiver, which can be assumed to be constant over at least one OFDM–symbol, and $n[k]$ represents the AWGN with variance $\sigma_n^2 = N_0 \cdot D \cdot \Delta f$ (see Section 2.2).

Applying the stochastic power line channel model of Section 2, the fading gain $g[k] \triangleq |s[k]|$ has for a fixed "time" k, or equivalently for a fixed subcarrier number ν, a Ricean distribution with the probability density function (pdf)[1] ($I_0(\cdot)$ is the modified Bessel function of order zero)

$$p_G(g|\nu) = \frac{2g}{\sigma_\nu^2} \cdot \exp\left(- \left(\frac{g^2}{\sigma_\nu^2} + K_\nu \right) \right) I_0\left(2g\sqrt{\frac{K_\nu}{\sigma_\nu^2}} \right) , \qquad (12)$$

where

$$\sigma_\nu^2 = \frac{P(\Delta f \cdot \nu)}{K_\nu + 1} \qquad (13)$$

and

$$K_\nu = \frac{m^2(\Delta f \cdot \nu)}{P(\Delta f \cdot \nu) - m^2(\Delta f \cdot \nu)} \qquad (14)$$

are the usual parameters of a Ricean pdf.

It is also interesting to consider the normalized channel state

$$\tilde{s}[k] \triangleq \frac{s[k]}{\sqrt{P(\Delta f \cdot k)} \cdot e^{-j\varphi_0(\Delta f \cdot k)}}$$

$$= \frac{s[k]}{\sqrt{(1 + K_k)\sigma_k^2} \cdot e^{-j\varphi_0(\Delta f \cdot k)}} , \qquad (15)$$

which corresponds to samples of the normalized transfer function from Equation (6). The normalized fading gain $\tilde{g}[k] \triangleq |\tilde{s}[k]|$ is Ricean distributed with parameters $\tilde{\sigma}^2$ and $\tilde{K}$ independent of the subcarrier number ν. Thus, the power line fading channel model for OFDM transmission is here constructed by using the well–known Ricean flat fading channel model and multiplying each channel gain $\tilde{g}[k]$ with the corresponding amplitude term $\sqrt{P(\Delta f \cdot k)}$.

Usually, adjacent OFDM-subcarriers are located within the coherence bandwidth B_c. Hence, the fading channel is slowly time–varying and the channel state can be expected to be constant over at least two consecutive symbols.

For transmission over a series of OFDM–symbols, we define the discrete–"time" stochastic process $s[\zeta, k]$, $k \in \mathbf{Z}$, as stochastic model for the fading channel, where ζ denotes the atomic event of the corresponding random experiment. Each sample function $s[\zeta, k]$ corresponds to one exemplary power line channel. Now, the long term time variance of the power line channel has to be taken into consideration, too. As a proven model to describe this time variance has not been established yet, one reasonable choice is that one realization of $s[\zeta, k]$ contains random variables of one sample function $H(\eta, f)$ for fixed frequency values $f = \Delta f \cdot \nu$, $\nu = 0, 1, \ldots, D - 1$. However, since we

---

[1] We denote random variables corresponding to signals by the respective capital letter.
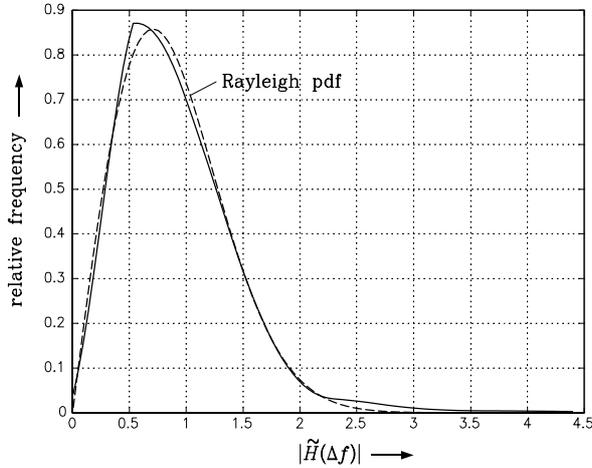
Fig. 3. Histogram of the normalized channel transfer function $|\tilde{H}(\Delta f \cdot \nu)|$ for $1 < (\Delta f \cdot \nu)/\text{MHz} < 4$ (solid line) and Rayleigh pdf (dashed line).

are interested in results which are valid for an average of power line transmission scenarios, it is more convenient to identify a sample function of $s[\zeta, k]$ with a concatenation of many realizations of the discrete–frequency stochastic process $H(\eta, \Delta f \cdot \nu)$, $\nu = k \bmod D$. In this case, one fading channel realization represents an ensemble average over power line channel realizations.

In order to provide a verification of this fading channel model, measurements of 10 channel transfer functions of one power line network [17] have been analyzed. Figure 3 shows the histogram of $|\tilde{H}(\Delta f \cdot \nu)|$ (solid line) for $1 < (\Delta f \cdot \nu)/\text{MHz} < 4$ assuming that the average power transfer function $P(f)$ is well approximated by equation (4), where the attenuation parameter a is fitted to the sample transfer functions. The subcarrier spacing Δf is chosen appropriately small so that a sufficient number of samples of $\tilde{H}(f)$ occurs in the histogram. Clearly, the fluctuations of the curve are due to the relatively small available data base. For a comparison the Rayleigh pdf, which is the special case of the Ricean pdf with Ricean parameter K equal to zero, is plotted in Figure 3 (dashed line). As can be seen, the pdf given by the stochastic model satisfactorily matches the histogram based on measurements.

4. Channel Capacity

Having established a fading channel model for power line communications using OFDM, we are now in the position to calculate channel capacities as figure of merit to compare different transmission schemes. It should be noted that the capacities are expressed as ensemble averages. Thus, the capacities represent averages of achievable rates over an ensemble of power line channel realizations and they are not the achievable rates for all special channel realizations.

Subsequently, we will distinguish the cases where information on the channel state and the carrier phase are and are not available at the receiver.

4.1   Coherent Transmission

The fading channel model introduced in Section 3 is applied and channel state information (CSI) is supposed to be available at the receiver side, i.e., the channel gain and phase are known. In this case, at least from the information theoretical point of view, the dependency between consecutive channel states, i.e., the channel memory, is of no importance. But usually, in order to make standard coding techniques applicable, interleaving at the transmitter and deinterleaving at the receiver are performed leading to a virtually memoryless channel between x and y. As full CSI is also passed through the deinterleaver, capacity is not affected by such an interleaving technique, of course. The corresponding system model for coherent transmission is sketched in Figure 4.

Fig. 4. System model for coherent transmission.

The channel is described by the conditioned pdf $p_Y(y|x, s, \varphi_c)$. Since coherent reception is assumed and since the noise is rotationally invariant, the phase of $s[k] \cdot \text{e}^{\text{j}\varphi_c}$ is irrelevant and it is sufficient to consider $p_Y(y|x, g)$. Clearly, $p_Y(y|x, g)$ is the well–known two–dimensional Gaussian pdf with mean $g[k] \cdot x[k]$.

The calculation of the channel capacity requires the optimization of all free parameters. As we are interested in the limits for given PSK and QAM signal constellations with uniformly, independently, and identically distributed (u.i.i.d.) signal points, i.e., constellation and a–priori probabilities are regarded as part of the channel, no optimization on these parameters has to be performed. For coherent reception and perfect channel state information, the capacity C_{CSI}, measured in bit per symbol, equals the average mutual information [18]

$$C_{\text{CSI}} = \mathcal{E}_{Y,X,G} \left\{ \log_2 \left(\frac{p_Y(y|x,g)}{p_Y(y|g)} \right) \right\}, \qquad (16)$$

where $p_Y(y|g)$ is the average pdf of the channel output given the channel state. For averaging over the channel state the pdf

$$p_G(g) = \frac{1}{D} \sum_{\nu=0}^{D-1} p_G(g|\nu) \qquad (17)$$

with $p_G(g|\nu)$ from (12) is used.

4.2   Noncoherent Transmission

In many communications scenarios reliable estimation of the channel state and carrier phase is not practicable. For such applications the use of differential encoding at the transmitter and noncoherent reception at the receiver are convenient. Figure 5 shows the system model for noncoherent transmission.

By differential encoding the information is conveyed in the transitions of the channel input symbols x. The current transmitted symbol $x[k]$ is determined by an interleaved version (discussed in detail below) of the data–
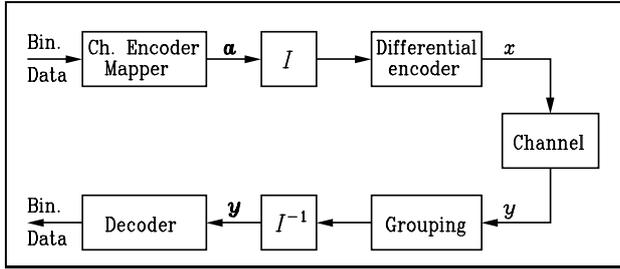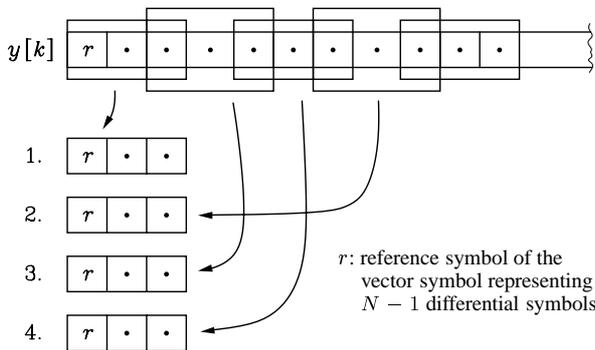
Fig. 5. System model for noncoherent transmission.

Fig. 6. Grouping of the received sequence $y[k]$ into overlapping vectors $\boldsymbol{y}$ of length $N = 3$ and deinterleaving.

carrying (differential) symbol $a[k]$ and the previous transmitted symbol $x[k-1]$. For high bandwidth efficiency this differential encoding is performed in both phase and amplitude, which is known as differential amplitude and phase shift keying (DAPSK), e.g. [19].

Suitable signal constellations are $\alpha A\beta PSK$ for the symbols x, which consist of $M = \alpha \cdot \beta$ points arranged in α distinct concentric rings with different radii ρ_i, $i = 0, 1, \ldots, \alpha - 1$, and β uniformly spaced phases φ_m, $m = 0, 1, \ldots, \beta - 1$, so–called "star–constellations" cf. [20]. As usual, the differential symbols a are taken from the same signal set as the transmitted signal. Let $i[k]$ and $m[k]$, $k \in \mathbf{Z}$, denote the sequences of radius and phase indices of the corresponding sequence $x[k]$ of channel symbols, i.e., $x[k] = \rho_{i[k]} e^{j\varphi_{m[k]}}$. Additionally, the radius and phase indices of the differential symbols $a[k]$ are written by $j[k]$ and $n[k]$, i.e, $a[k] = \rho_{j[k]} e^{j\varphi_{n[k]}}$. Then, differential encoding is performed by

$$ x[k] = \rho_{(i[k-1]+j[k]) \bmod \alpha} e^{j\varphi_{(m[k-1]+n[k]) \bmod \beta}} . \quad (18) $$

In conventional differential detection the discrete channel output sequence $y[k]$ is partitioned into overlapping vectors $\boldsymbol{y}$ of two consecutive symbols at the receiver. If the coherence bandwidth of the channel is (at least) $N > 2$ symbols the receiver favorably operates on blocks $\boldsymbol{y}$ of $N > 2$ consecutive symbols, overlapping each other by one symbol, see Figure 6 (where $N = 3$) and cf. e.g. [21]. This multiple symbol differential detection provides further gains, e.g. [21, 22].

From the observation of one received vector $\boldsymbol{y}$, decision variables on the differential vector $\boldsymbol{a}$ of $N - 1$ data sym-

bols a are obtained. Thereby, $\boldsymbol{y}$ corresponds to the vector $\boldsymbol{x}$ containing N transmitted symbols x, where the first entry acts as reference symbol r of the differential encoder. In order to apply standard coding techniques for memoryless channels, it is convenient to ignore the statistical dependencies between the blocks $\boldsymbol{y}$. This is generated by applying (asymptotically ideal) interleaving based on vector symbols $\boldsymbol{a}$ and $\boldsymbol{y}$, respectively, which generates a virtually memoryless channel between $\boldsymbol{a}$ and $\boldsymbol{y}$. Figure 6 illustrates overlapping, grouping, and deinterleaving for $N = 3$. Although the current channel gains $g[k]$ are assumed to be unknown to the receiver, it is reasonable to exploit the well–known average channel parameters σ_ν^2 and K_ν introduced in (13) and (14), respectively, for each OFDM–subcarrier $\nu = 0, 1, \ldots, D - 1$. Here, each vector symbol $\boldsymbol{a}$ and $\boldsymbol{y}$, respectively, corresponds to N subcarriers. Since a verified model of the acf of the channel gain has not been found yet, we employ the usual assumption that the channel gain is almost constant over (at least) N subcarriers. Thus, the memoryless channel is represented by the pdf $p_{\boldsymbol{Y}}(\boldsymbol{y}|\boldsymbol{a}, \nu)$, where the dependency on σ_ν^2 and K_ν is expressed by conditioning on one subcarrier number ν of the N consecutive subcarriers.

In order to determine $p_{\boldsymbol{Y}}(\boldsymbol{y}|\boldsymbol{a}, \nu)$ the fading channel input–output–relation (11) is extended to vector symbols

$$ \boldsymbol{y}[\ell] = s[\ell] \cdot e^{j\varphi_c} \cdot \boldsymbol{x}[\ell] + \boldsymbol{n}[\ell] , \quad (19) $$

where $s[\ell]$ is nearly equal for all components of $\boldsymbol{x}[\ell]$, $\boldsymbol{n}[\ell]$ denotes independent AWGN with variance $\sigma_n^2 = N_0 \Delta f D$ per complex component, and $\ell = \lfloor k/(N-1) \rfloor \in \mathbf{Z}$ denotes the discrete–"time" index corresponding to vector symbols. The pdf $p_{\boldsymbol{Y}}(\boldsymbol{y}|\boldsymbol{x}, \nu)$ is derived in [21, Appendix]. Replacing $\boldsymbol{x}$ by $\boldsymbol{a}$ and one reference symbol r according to (18), $p_{\boldsymbol{Y}}(\boldsymbol{y}|\boldsymbol{x}, \nu)$ can be expressed by $p_{\boldsymbol{Y}}(\boldsymbol{y}|\boldsymbol{a}, r, \nu)$. This pdf includes inversion of the differential encoding. Averaging this pdf over all possible reference symbols r finally yields the desired pdf $p_{\boldsymbol{Y}}(\boldsymbol{y}|\boldsymbol{a}, \nu)$.

Now, the capacity of the memoryless vector channel, normalized to bit per scalar symbol, is calculated by

$$ C(N) = \frac{1}{N-1} \cdot \frac{1}{D} \sum_{\nu=0}^{D-1} \mathcal{E}_{\boldsymbol{Y}, \boldsymbol{A}} \left\{ \log_2 \left(\frac{p_{\boldsymbol{Y}}(\boldsymbol{y}|\boldsymbol{a}, \nu)}{p_{\boldsymbol{Y}}(\boldsymbol{y}|\nu)} \right) \right\} . \quad (20) $$

It should be noted that no optimization of the distribution of $\boldsymbol{a}$ can be performed. Regardless the distribution of $\boldsymbol{a}$ the differentially encoded symbols x will be uniformly distributed. Therefore, we had already restricted the differential symbols $\boldsymbol{a}$ to be u.i.i.d., which maximizes the throughput of the channel.

5. Numerical Results

In this section capacities over the average signal–to–noise ratio $\bar{E}_s/N_0$ ($\bar{E}_s$: average receive energy per symbol) are evaluated by numerical integration. The results are independent of the number D of OFDM–subcarriers and the subcarrier spacing Δf as long as $N \cdot \Delta f \ll B_c$ holds.

For the following numerical results we suppose the channel gains $g[k]$ corresponding to subcarriers $\nu = k \bmod D$ to be Rayleigh distributed, which is the most important special case of the Ricean fading model. The average power transfer function $P(f)$ with exponential decay

in f is used, cf. (4), i.e.,

$$\sigma_\nu^2 = P(\Delta f \cdot \nu) \propto \exp\left(-a \cdot \Delta f \cdot \nu\right) \ . \qquad (21)$$

The attenuation parameter a is set to 10^{-7} 1/Hz and 10^{-6} 1/Hz, respectively, typical for some classes of power line channels. Their orders of magnitude coincide with the parameters of sample networks given in [8]. Furthermore, the transmission bandwidth B_T is assumed to be limited to 2 MHz and 3 MHz, respectively, which are reasonable values regarding restrictions imposed on power line communications by regulator authorities [23]. It should be noted that the capacity in bit per channel use versus $\bar{E}_s/N_0$ depends on the transmission bandwidth because, via the average power transfer function $P(f)$, the channel fading properties depend on B_T. Although the channel parameters are only exemplary chosen, the subsequently drawn consequences apply in general.

5.1   Coherent Transmission

Coherent transmission with perfect channel state information and usual 4PSK, 8PSK, 16QAM, 32QAM, and 64QAM providing spectral efficiencies up to 6 bit/s/Hz is considered.

Figure 7 presents the capacity curves for $a = 10^{-7}$ 1/Hz and $B_T = 3$ MHz. As reference, the respective capacities of the AWGN channel are shown. As expected, for a fixed information rate, the fading channel of OFDM transmission over power lines requires a considerably higher SNR than the AWGN channel. Furthermore, it is interesting to recognize that for the AWGN channel the curves of different signal constellations converge much faster towards lower capacity values than for the fading channel. Hence, in terms of capacity it is advantageous to spend more than one bit of redundancy per complex symbol (cf. [24]), i.e., larger signal constellations in combination with low rate codes are favorably used. The same observation based on bit error rates has also been reported in [5], where this strategy is called channel symbol expansion diversity (CSED).

In Figure 8 the influence of the parameter a on the capacity is illustrated. As can be seen, the capacity at a certain SNR decreases for the larger value of a. Whereas in the case of $a = 10^{-7}$ 1/Hz the fading variances σ_ν^2 are almost identical for all ν, and hence, the channel is essentially Rayleigh fading ($p_G(g)$ in (17) is the Rayleigh pdf), for $a = 10^{-6}$ 1/Hz the variances vary strongly over the subchannel number, and thus, the channel gain fluctuates more heavily. Regarding the capacity curves of different constellations the concept of CSED is expected to provide higher gains for increasing a.

Concerning the capacity over the average SNR, using a larger transmission bandwidth is equivalent to increasing the value of a. Figure 9 shows the capacity curves for $B_T = 2$ MHz and $B_T = 3$ MHz. For a bandwidth of 3 MHz the channel gain performs a stronger fading which leads to a performance loss compared to the case of $B_T = 2$ MHz. Therefore, as long as $\exp(-a \cdot f)$ does not deviate negligibly from one, relatively large signal constellations should be applied for power line transmission over a wide spectral range. Although the capacity in bit per channel use decreases for increasing transmission bandwidth B_T due to more severe fading, transmission capacity measured in bit per second increases with increasing
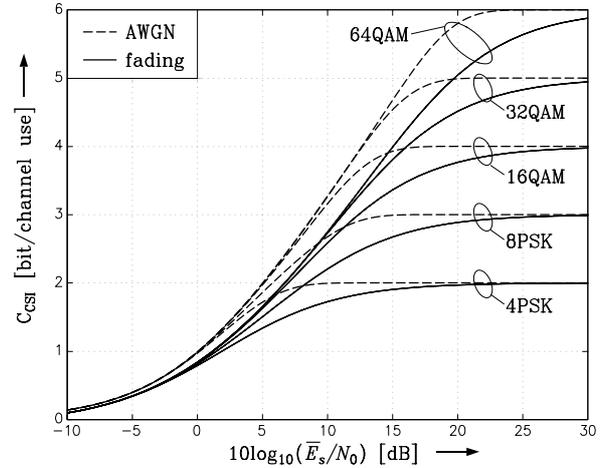

Fig. 7. Capacities C_{CSI} (coherent reception) for 4PSK, 8PSK, 16QAM, 32QAM, 64QAM. Solid lines: Fading channel of OFDM over power lines with parameters $a = 10^{-7}$ 1/Hz and $B_T = 3$ MHz. Dashed lines: AWGN channel.
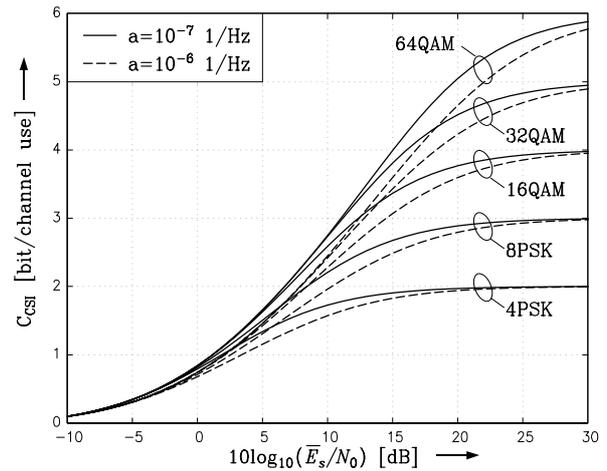

Fig. 8. Capacities C_{CSI} (coherent reception) for 4PSK, 8PSK, 16QAM, 32QAM, 64QAM. Fading channel of OFDM over power lines with $B_T = 3$ MHz. Solid lines: $a = 10^{-7}$ 1/Hz. Dashed lines: $a = 10^{-6}$ 1/Hz.

B_T because of a higher possible number of channel uses per second, of course.

5.2   Noncoherent Transmission

Differentially encoded transmission and differential detection is regarded without channel state information. The rings of the DαAβPSK constellations are geometrically spaced with the ratios $\rho_1/\rho_0 = 2$ for $\alpha = 2$ and $\rho_{i+1}/\rho_i = 1.4$, $i = 0, 1, 2$ for $\alpha = 4$, which were found to be advantageous for fading channels [25, 26]. Note, optimally the ring ratios have to be optimized for each SNR.

Figure 10 comprises the capacity curves of various αAβPSK constellations, which offer spectral efficiencies up to 6 bit/s/Hz, and noncoherent detection with
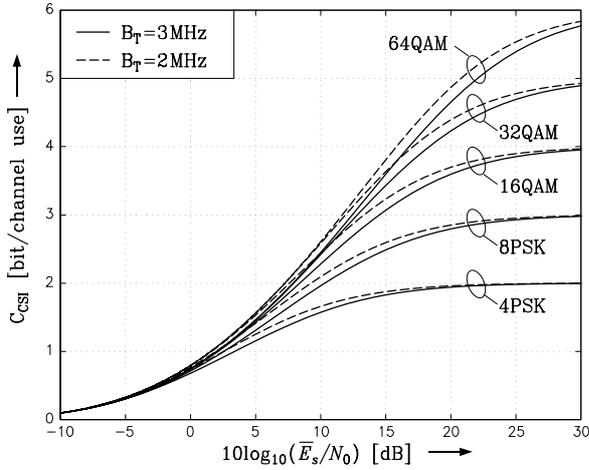
AEÜ Int. J. El. Commun.
(1999) No. x, 1–1

Lampe, Huber: Bandwidth Efficient Power Line Communications Based on OFDM   7

Fig. 9. Capacities C_{CSI} (coherent reception) for 4PSK, 8PSK, 16QAM, 32QAM, 64QAM. Fading channel of OFDM over power lines with $a = 10^{-6}$ 1/Hz. Solid lines: $B_{\mathrm{T}} = 3$ MHz. Dashed lines: $B_{\mathrm{T}} = 2$ MHz.
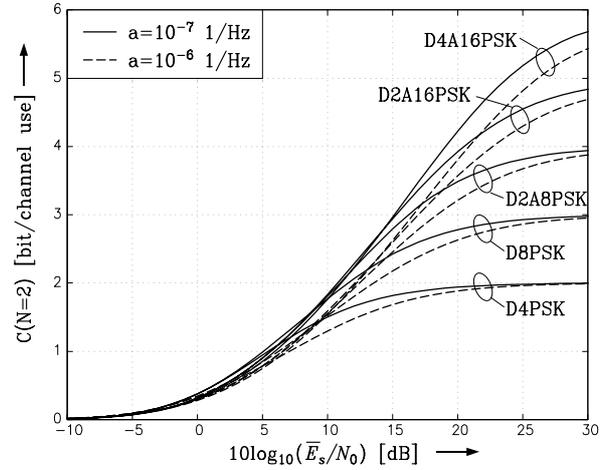

Fig. 10. Capacities $C(N = 2)$ (conventional differential reception) for D4PSK, D8PSK, D2A8PSK, D2A16PSK, D4A16PSK. Solid lines: Fading channel of OFDM over power lines with parameters $a = 10^{-7}$ 1/Hz and $B_{\mathrm{T}} = 3$ MHz. Dashed lines: $a = 10^{-6}$ 1/Hz.

$N = 2$. The parameters of the power line channel are $a = 10^{-7}$ 1/Hz and $a = 10^{-6}$ 1/Hz, respectively, and $B_{\mathrm{T}} = 3$ MHz. Since the ring ratios are fixed, the capacity curves for DAPSK and DPSK intersect. Consequently, CSED is not expected to provide gains for relatively low target rates, e.g., 2 bit/ch.use for $a = 10^{-7}$ 1/Hz. However, if high spectral efficiencies are desired, gains can be achieved by spending more than one bit of redundancy per symbol. Moreover, for increasing a the positive effect of CSED intensifies. Similar to the case of coherent transmission, the capacity loss due to fading strongly depends on the parameter a (For clarity, the respective capacity curves of the AWGN channel are omitted in Figure 10.).

In order to assess the performance loss because of differential detection, Figure 11 displays the capacities for coherent and noncoherent transmission with 16QAM and D2A8PSK, respectively. In the case of conventional differential detection, i.e., $N = 2$, a loss of 3 to 5 dB of signal–to–noise ratio for differentially encoded transmission compared to coherent transmission is recognizable. By applying multiple symbol differential detection this gap can be compensated in part as shown in Figure 11 for $N = 3, 4$. If N approaches infinity the normalized capacity $C(N)$ converges to C_{CSI}, cf. [27].

6. Simulation Results

In order to further assess the capabilities of power line communications, different transmission scenarios have been simulated. In particular, 8PSK and 16QAM transmission with coherent reception and perfect channel state information at the receiver and 8PSK differentially encoded transmission (D8PSK) with (conventional) differential detection for $N = 2$ over the power line fading channel are considered. Again, the Rayleigh fading model for the subchannel transfer factors with variances according to equation (21) is used. The attenuation parameters are chosen $a = 10^{-6}$ 1/Hz and $a = 10^{-7}$ 1/Hz, respectively, and transmission bandwidth is $B_{\mathrm{T}} = 3$ MHz .
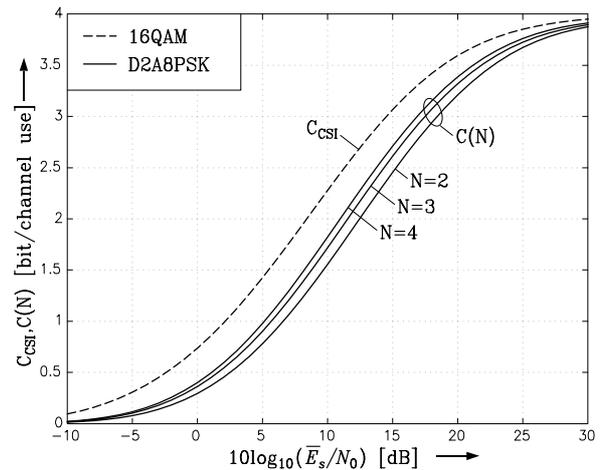

Fig. 11. Capacities C_{CSI} and $C(N)$ for 16QAM and D2A8PSK, respectively. Fading channel of OFDM over power lines with $a = 10^{-6}$ 1/Hz and $B_{\mathrm{T}} = 3$ MHz. Solid lines: $C(N = 2, 3, 4)$ (from right to left). Dashed lines: C_{CSI}.

As coded modulation scheme we apply bit–interleaved coded modulation (BICM) [28, 29] in combination with Gray labeling of the signal points. BICM is a suboptimum but simple scheme applying only one binary code. For several applications it has been shown [29] that based on Gray labeling BICM suffers only a marginal capacity loss compared to optimum coded modulation via multilevel coding (MLC) with multistage decoding (MSD) [30, 31].

Parallel concatenated convolutional codes (Turbo codes) [3] perform close to the capacity limit and are thus used as codes. We employ Turbo codes with 16 state constituent codes and random interleavers. The symmetrical decoder concept according to [32] is used. Rate is adjusted by symmetric puncturing of parity symbols, cf. [32]. In the decoding 6 iterations are executed.

The code lengths are chosen in that way that the code symbols of one code word are mapped to 1000 channel symbols. As the use of $D \gtrsim 1000$ subcarriers is practical regarding the bandwidth of 3 MHz, coding can be done separately for each OFDM–symbol. If (bit)interleaving is also restricted to one OFDM–symbol, the transmission delay is limited to 1000 channel symbols. However, in order to obtain results that are not affected by the special choice of the autocorrelation function $\phi_{\bar{H}\bar{H}}(f)$ (cf. Section 2.1), for which a proved model does not exist, ideal symbol interleaving is simulated by generating the subchannel transfer factors λ_ν, $\nu = 0, 1, \ldots, D-1$, independently of each other. If the coherence bandwidth of the power line channel is negligible compared to the interleaving depth, this model is appropriate. In all simulations, the bit–interleavers are randomly generated in order to provide results independent of a particular chosen interleaver.

In Figure 12 the bit error rates (BER) of coherent transmission using 16QAM and 8PSK for a target rate equal to 2.0 bit/symbol are compared. The lengths of the binary codes are 4000 for 16QAM and 3000 for 8PSK, respectively, i.e., 1000 OFDM–subcarriers are active. Ideal interleaving is applied as indicated above. As reference, the capacity limits taking the finite error rate into account ("rate–distortion capacities") [33] are shown. As can be seen, 16QAM clearly outperforms 8PSK. This is due to the higher constellation expansion diversity when 16QAM with code rate 1/2 is applied to achieve the desired target rate of 2.0 bit/symbol. The gap of about 1.5 dB between the curves simulated for 8PSK and 16QAM matches the result predicted by the capacity analysis, which is illustrated by the rate–distortion capacities. For BER's around 10^{-4} the gap between the required signal–to–noise ratios and the capacity limits is about 2 dB.

Coherent transmission with 16QAM over power line channels with different attenuation parameters a is regarded in Figure 13. Clearly, the stronger fading due to a larger value of a leads to a performance loss. In particular, the power efficiency decreases by about 1.7 dB when a increases from 10^{-7} 1/Hz to 10^{-6} 1/Hz. Again, the simulation results are in great accordance with the rate–distortion capacities.

As mentioned in Section 4.1, the channel memory does not play any role for the capacity of the coherent transmission scheme. But if the channel coherence bandwidth is relatively large and interleaving is done within one OFDM–symbol, a decoding error is caused with high probability when deep fades occur, which leads to an increased average error rate. In order to study these effects in more detail, we use a simple model for the normalized stationary Gaussian process $\tilde{H}(\eta, f)$, i.e., a Gaussian acf

$$\phi_{\bar{H}\bar{H}}(f) = \exp(-\pi(f/B_{\mathrm{c}})^2) . \qquad (22)$$

The simulation results for different values of the coherence bandwidth B_{c} are depicted in Figure 14 ($a = 10^{-7}$ 1/Hz, $B_{\mathrm{T}} = 3$ MHz). Again, randomly generated bit–interleavers are applied. The curves show that the channel memory cannot completely be eliminated by the (bit)interleaving within one OFDM–symbol, i.e, for a larger B_{c} the bit error rate deteriorates. For the coherence bandwidths comprising 5 and 11 OFDM–subchannels, respectively, the losses in power efficiency are about 0.2 dB and 0.6 dB, respectively, for BER $\approx 10^{-4}$. Although the interleaving depth of 1000 channel symbols is still rela-
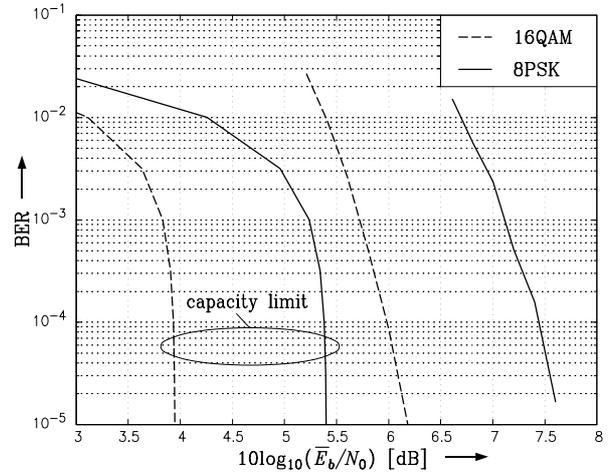

Fig. 12. BER as a function of $\bar{E}_b/N_0$ for coherent transmission with 8PSK (solid lines) and 16QAM (dashed lines) and rate 2.0 bit/symbol. Fading channel of OFDM over power lines with $a = 10^{-7}$ 1/Hz and $B_{\mathrm{T}} = 3$ MHz. Channel coding over one OFDM–symbol. BICM with ideal interleaving. Left hand side: respective rate–distortion capacity limits.
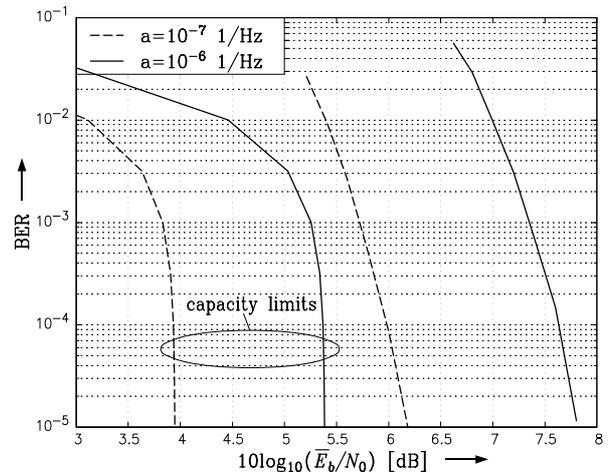

Fig. 13. BER as a function of $\bar{E}_b/N_0$ for coherent transmission with 16QAM and rate 2.0 bit/symbol. Fading channel of OFDM over power lines with $B_{\mathrm{T}} = 3$ MHz and $a = 10^{-6}$ 1/Hz (solid lines) and $a = 10^{-7}$ 1/Hz (dashed lines), respectively. Channel coding over one OFDM–symbol. BICM with ideal interleaving. Left hand side: respective rate–distortion capacity limits.

tively large when compared to the coherence bandwidth of e.g. 11 channel symbols, this effect occurs because of the high sensitivity of the Turbo code to statistical dependencies within the received symbol sequence.

Finally, coherent transmission with channel state information and differentially encoded transmission without channel state information using the 8PSK signal constellation are compared. Here, ideal interleaving is simulated, and for D8PSK the channel is assumed to be constant over two consecutive symbols. The target rate of 1.5 bit/symbol is chosen. In Figure 15 the simulation results are plotted.
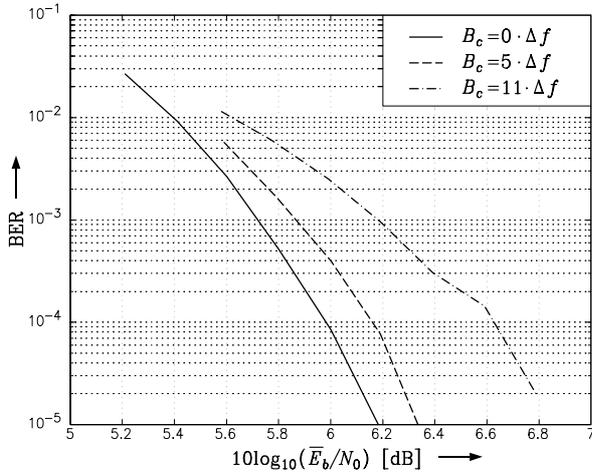
AEÜ Int. J. El. Commun.
(1999) No. x, 1–1

Lampe, Huber: Bandwidth Efficient Power Line Communications Based on OFDM   9

Fig. 14. BER as a function of $\bar{E}_b/N_0$ for for coherent transmission with 16QAM and rate 2.0 bit/symbol. Fading channel of OFDM over power lines with $a = 10^{-7}$ 1/Hz and $B_T = 3$ MHz. Autocorrelation function $\phi_{\tilde{H}\tilde{H}}(f)$ according to (22). Coherence bandwidth: $B_c = 0$ Hz (solid line), $B_c = 5 \cdot \Delta f$ (dashed line), $B_c = 11 \cdot \Delta f$ (dash–dotted line). BICM (channel coding and random interleaving) over one OFDM–symbol.
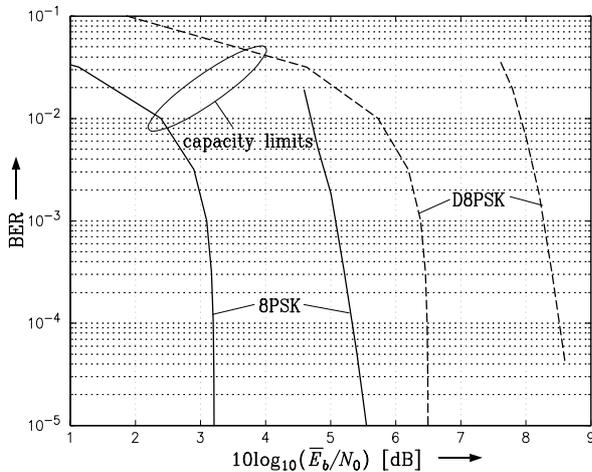

Fig. 15. BER as a function of $\bar{E}_b/N_0$ for 8PSK (solid lines) and D8PSK transmission and differential detection with $N = 2$ (dashed lines) and rate 1.5 bit/symbol. Fading channel of OFDM over power lines with $B_T = 3$ MHz and $a = 10^{-7}$ 1/Hz. Channel coding over one OFDM–symbol. Ideal interleaving. Left hand side: respective rate–distortion capacity limits.

As predicted by the theoretical considerations, a difference in the power efficiencies of about 3 to 3.5 dB between coherent and noncoherent transmission can be observed. An increase of the observation interval with $N > 2$ is expected to reduce the gap. But it should be noted that for $N > 2$ BICM is not the appropriate scheme [34].

7. Conclusions

In this paper power line communication systems employing OFDM are described and compared. Channel information is assumed not to be available at the transmitter side. Both the situations with and with no channel information at the receiver are regarded.

In order to make a general analysis possible a stochastic power line channel model is introduced. Incorporating the transmitter and receiver operations of OFDM into the model and using coding across the OFDM–subcarriers a slowly time–varying frequency non–selective fading channel is obtained. The capacity of this fading channel is calculated for the cases of coherent transmission and differentially encoded transmission with multiple symbol differential detection.

The numerical results of the channel capacity show that the frequency dependent signal attenuation and the transmission bandwidth largely influence the required average signal–to–noise ratio for reliable communication at the receiver. To combat the signal fading the application of large signal constellations and low rate codes proves to be convenient.

According to the capacity curves the perfect knowledge of the channel characteristic leads to considerable gains of the order of some dB in the signal–to–noise ratio. Increasing the observation interval of the noncoherent detection can reduce the gap between transmission with and with no channel state information at the receiver.

The theoretical results derived from capacity analysis are affirmed by means of simulations for 8PSK and 16QAM signal constellations. As well–known for transmission over fading channels, the interleaving depth is required to largely exceed the coherence bandwidth of the fading process along the frequency axis.

References

[1] J.A.C. Bingham. Multicarrier Modulation for Data Transmission: An Idea Whose Time Has Come. *IEEE Communications Magazine*, pages 5–14, May 1990.

[2] R. Fischer and J. Huber. On the equivalence of single- and multicarrier modulation: A new view. In *Proc. of IEEE Int. Symp. on Inf. Theory (ISIT)*, page 197, Ulm, June/July 1997.

[3] C. Berrou and A. Glavieux. Near Optimum Limit Error Correcting Coding and Decoding: Turbo–Codes. *IEEE Trans. on Commun.*, 44:1261–1271, October 1996.

[4] D. Divsalar and M.K. Simon. Multiple–Symbol Differential Detection of MPSK. *IEEE Trans. on Commun.*, 38(3):300–308, March 1990.

[5] U. Hansson and T. Aulin. Channel Symbol Expansion Diversity - Improved Coded Modulation for the Rayleigh Fading Channel. In *Proc. of IEEE Int. Conf. on Commun. (ICC)*, pages 891–895, Dallas, August 1996.

[6] L.E. Franks. Carrier and Bit Synchronisation in Data Communication—A Tutorial Review. *IEEE Trans. on Commun.*, 28(8):1107–1121, August 1980.

[7] M. Arzberger, K. Dostert, T. Waldeck, and M. Zimmermann. Fundamental Properties of the Low Voltage Power Distribution Grid. In *Proc. of Int. Symp. on Power Line Commun. and its Appl. (IS-PLC)*, pages 45–50, Essen, Germany, April 1997.

[8] M. Zimmermann and K. Dostert. A Multi–Path Signal Propagation Model for the Power Line Channel in the High Frequency Range. In *Proc. of Int. Symp. on Power Line Commun. and its Appl. (IS-PLC)*, pages 45–51, Lancaster, UK, March 1999.

[9] H. Philipps. Modelling of Powerline Communications Channels. In *Proc. of Int. Symp. on Power Line Commun. and its Appl. (ISPLC)*, pages 14–21, Lancaster, UK, March 1999.

[10] A. Papoulis. *Probability, Random Variables, and Stochastic Processes*. McGraw–Hill, New York, third edition, 1991.

[11] K.M. Dostert. Telecommunications over the Power Distribution Grid - Possibilities and Limitations. In *Proc. of Int. Symp. on Power Line Commun. and its Appl. (ISPLC)*, pages 1–9, Essen, April 1997.

[12] O.G. Hooijen. A Channel Model for the Low–Voltage Power–Line Channel; Measurement and Simulation Results. In *Proc. of Int. Symp. on Power Line Commun. and its Appl. (ISPLC)*, pages 51–56, Essen, April 1997.

[13] P.S. Chow, J.M. Cioffi, and J.A.C. Bingham. A Practical Discrete Multitone Transceiver Loading Algorithm for Data Transmission over Spectrally Shaped Channels. *IEEE Trans. on Commun.*, 43:773–775, February/March/April 1995.

[14] R. Fischer and J. Huber. A new loading algorithm for discrete multitone transmission. In *Proc. of IEEE Global Telecom. Conf. (Globecom)*, pages 724–728, London, November 1996.

[15] A. Leke and J.M. Cioffi. A maximum rate loading algorithm for discrete multitone modulation systems. In *Proc. of IEEE Global Telecom. Conf. (Globecom)*, pages 1514–1518, Phoenix,Arizona, November 1997.

[16] M. Bossert, A. Donder, and V. Zyablov. OFDM–Übertragung über Mobilfunkkanäle: Bemerkungen zur Kanalkapazität (in German). In *2. OFDM–Fachgespräch*, Braunschweig, Germany, September 1997.

[17] Universität Erlangen-Nürnberg Lehrstuhl für Nachrichtentechnik II. Internal Report. 1998.

[18] R.G. Gallager. *Information Theory and Reliable Communication*. John Wiley & Sons, New York, 1968.

[19] A. Svensson. On Differentially Encoded Star 16QAM with Differential Detection and Diversity. *IEEE Trans. on Vehic. Technology*, 44(3):586–593, August 1995.

[20] W.T. Webb, L. Hanzo, and R. Steele. Bandwidth Efficient QAM Schemes for Rayleigh Fading Channels. *IEE Proceedings–I*, 138(3):169–175, June 1991.

[21] D. Divsalar and M.K. Simon. Maximum-Likelihood Differential Detection of Uncoded and Trellis Coded Amplitude Phase Modulation over AWGN and Fading Channels — Metrics and Performance. *IEEE Trans. on Commun.*, 42(1):76–89, January 1994.

[22] L. Lampe, S. Calabrò, and R. Fischer. Channel Capacity of Fading Channels for Differentially Encoded Transmission. *IEE Electronics Letters*, 35(3):192–194, February 1999.

[23] M. Harris. Power Line Communications—A Regulatory Perspective. In *Proc. of Int. Symp. on Power Line Commun. and its Appl. (ISPLC)*, pages 131–138, Lancaster, UK, March 1999.

[24] G. Ungerböck. Channel Coding with Multilevel/Phase Signals. *IEEE Trans. on Inf. Theory*, 28(1):55–67, January 1982.

[25] L. Lampe and R. Fischer. Comparison and Optimization of Differentially Encoded Transmission on Fading Channels. In *Proc. of Int. Symp. on Power Line Commun. and its Appl. (ISPLC)*, pages 107–113, Lancaster, UK, March 1999.

[26] C.D. Chung. Differentially Amplitude and Phase–Encoded QAM for the Correlated Rayleigh–Fading Channel with Diversity Reception. *IEEE Trans. on Commun.*, 45(3):309–321, March 1997.

[27] R.J. McEliece and W.E. Stark. Channels with Block Interference. *IEEE Trans. on Inf. Theory*, 30(1):44–53, January 1984.

[28] Ephraim Zehavi. 8–PSK Trellis Codes for a Rayleigh Channel. *IEEE Trans. on Commun.*, 40(5):pp. 873–884, May 1992.

[29] Giuseppe Caire, Giorgio Taricco, and Ezio Biglieri. Bit–Interleaved Coded Modulation. *IEEE Trans. on Inf. Theory*, 44(3):pp. 927–946, May 1998.

[30] H. Imai and S. Hirakawa. A New Multilevel Coding Method Using Error Correcting Codes. *IEEE Trans. on Inf. Theory*, 23:371–377, 1977.

[31] U. Wachsmann, R. Fischer, and J. Huber. Multilevel Codes: Theoretical Concepts and Practical Design Rules. *IEEE Trans. on Inf. Theory*, pages 1361–1391, July 1999.

[32] U. Wachsmann and J. Huber. Power and bandwidth efficient digital communication using turbo codes in multilevel codes. *European Trans. on Telecommun.*, vol. 6:pages 557–567, Sept.–Oct. 1995.

[33] S.A. Butman and R.J. McEliece. The Ultimate Limits of Binary Coding for a Wideband Gaussian Channel. *JPL Deep Space Network Progress Report 42–22*, pages 78–80, August 1974.

[34] L. Lampe, S. Calabrò, R. Fischer, S. Müller-Weinfurtner, and J. Huber. On the Difficulty of Bit-Interleaved Coded Modulation for Differentially Encoded Transmission. In *Proc. of IEEE Inf. Theory Workshop (ITW)*, page 111, Kruger National Park, SA, June 1999.

Lutz Lampe was born in Leipzig, Germany, in 1973. He received the Dipl.–Ing. degree in electrical engineering from the University of Erlangen–Nürnberg in 1998. He is now a Research Assistant at the Telecommunications Institute at the University of Erlangen–Nürnberg. Currently, his research is focused on high–rate digital transmission over power line distribution networks. His interests comprise general issues of information theory and digital communications, and especially multi-carrier modulation and differentially encoded transmission.

Johannes Huber received the Diplom (Univ.) degree from the Technical University of Munich, the Ph.D. degree and habilitation degree (Dr.–Ing. habil.) in electrical engineering from the Federal Armed Forces University in Munich–Neubiberg in 1977, 1982, and 1991, respectively. From 1982 to March 1991, he was chief engineer at the Telecommunications Institute of the Federal Armed Forces University in Munich–Neubiberg and a lecturer in digital communications and coding. In parallel, he was a lecturer at the university of applied science in Munich. In 1991, he was a Visiting Scientist at the IBM Zurich Research Laboratory performing joint work with Dr. G. Ungerboeck. Since November 1991, he is a full professor for communication engineering at the University of Erlangen–Nürnberg, Germany. Since August 1997, he is head of the Telecommunications Institute II and of the Telecommunications Laboratory of the University of Erlangen–Nürnberg. Johannes Huber is member of the editorial boards of the International Journal of Electronics and Communications (AEÜ, since 1993) and IEEE Trans. on Communications (since 1996). Since May 1998, he is Editor–in–Chief of the AEÜ. His research interests are all sorts of applications of Information Theory, especially power and bandwidth efficient digital communications and channel coding. Johannes Huber is author or co–author of about 95 articles and conference papers and of a textbook "Trelliscodierung" (in German). In 1988, he received the research award of the German Society of Information Techniques (ITG).